

PAPER

Study of the vortex based virtual valve micropump

To cite this article: Tao Wang *et al* 2018 *J. Micromech. Microeng.* **28** 125007

View the [article online](#) for updates and enhancements.



IOP | ebooks™

Bringing you innovative digital publishing with leading voices to create your essential collection of books in STEM research.

Start exploring the collection - download the first chapter of every title for free.

Study of the vortex based virtual valve micropump

Tao Wang^{1,2} , Jian He^{1,2}, Chunquan An^{1,2}, Jiejun Wang^{1,2}, Lu Lv^{1,2}, Wenbo Luo^{1,2}, Chuangui Wu^{1,2}, Yao Shuai^{1,2}, Wanli Zhang^{1,2} and Chengkuo Lee³ 

¹ School of Electronic Science and Engineering, University of Electronic Science and Technology of China, 2006 Xiyuan Avenue, Chengdu 611731, People's Republic of China

² State Key Laboratory of Electronic Thin Film and Integrated Devices, University of Electronic Science and Technology of China, 2006 Xiyuan Avenue, Chengdu 611731, People's Republic of China

³ Department of Electrical and Computer Engineering, National University of Singapore, 4 Engineering Drive 3, Singapore 117583, Singapore

E-mail: t.wang@uestc.edu.cn

Received 22 June 2018, revised 29 September 2018

Accepted for publication 11 October 2018

Published 1 November 2018



Abstract

The research and development of piezoelectric valve-less micropumps have become an increasingly popular topic for decades. A highly efficient valve-less micropump is necessary to deliver liquids for microfluidic control systems. Study of the flow mechanism in the valve-less micropump may help to further improve the pumping efficiency. In this paper, a dynamic finite element model is used to investigate the mechanism of a valve-less micropump with a diffuser/nozzle. The simulation result shows that the flow performance of a valve-less micropump is not only dependent on the diffuser/nozzle but is also related to the entire structure. When fluid flows through the nozzle, the chamber connected to the nozzle end is considered as a diffuser with an angle of 180°. This diffuser is located in the jet flow region, where the high velocity fluid generates a vortex in the interfacial area of the nozzle and chamber. Such a vortex works as a 'virtual valve', which can block the reflux and result in unidirectional flow. Besides, the vortex degree is tightly related to fluid velocity, which is determined by the input voltage. When the input voltage is larger than the threshold voltage (20 V), the virtual valve is activated, and the flow rate of the micropump increases rapidly with the input voltage. The simulation analysis conclusions are verified by experiment results. The experimental results demonstrate that the maximum flow rate of 5.4 ml min⁻¹ is finally obtained, which is comparable to a typical valve micropump.

Keywords: valve-less micropump, vortex, virtual valve, 3D printing technology

(Some figures may appear in colour only in the online journal)

1. Introduction

As a necessary component of a microfluidic control system [1], the micropump transforms electric energy, heat energy or mechanical energy into fluid kinetic energy. A piezoelectric micropump employs a piezoelectric actuator to transform electric energy into mechanical deformation [2]. As piezoelectric actuation can provide a high actuation force and fast mechanical response, a piezoelectric micropump presents several advantages such as having small dimensions, low power

consumption, and integrating easily. Therefore, piezoelectric micropumps receive considerable attention from researchers for wide applications in biomedical devices [3], drug delivery, blood analysis, biological and chemical analysis [4], micro-electronic cooling, fuel-drop generators for automobile heaters, environmental monitoring systems [5], and space exploration [6]. According to the rectifying mechanism, piezoelectric micropumps can be classified into valve piezoelectric pumps and valve-less piezoelectric pumps [3]. Even though valve-less micropumps may not completely block

the backward flow, valve-less micropumps have advantages of high reliability [7, 8], simple structure and miniaturization compared to valve micropumps [9, 10]. Hence, they attract widespread attention, and various studies on the characteristics of valve-less micropumps have been conducted [9, 11, 12].

Previous researchers believe the diffuser/nozzle structure is the key part of a valve-less micropump. Olsson *et al* [13, 14] propose that the diffuser has a low velocity in the outlet but low pressure loss, which leads to small flow resistance. On the contrary, the nozzle has the opposite function and results in high flow resistance. The flow resistance coefficient and diffuser efficiency are referred as the pumping efficiency of the diffuser/nozzle [15, 16]. Moreover, the stability map of the diffuser is presented by Wei [17] to systematically study the fluidic characteristics of the diffuser. The researchers point out the diffuser should be in the transitory stall region to achieve the lowest flow resistance.

These conclusions have been generally accepted for decades [15, 18, 19]. However, the diffuser/nozzle may not be sufficient to describe the behaviour of the micropump. In this research, the entire valve-less micropump structure is taken into account. A dynamic finite element model (FEM) for studying the mechanism of a valve-less micropump is also developed. The simulation result shows that a vortex may emerge in the interfacial region of the nozzle end and chamber. The induced vortex could work like a virtual valve, which significantly blocks the backflow. The vortex grade is highly related to the fluid velocity, which is determined by the driving voltage of the piezoelectric actuator. A vortex starts emerging at 20 V, which is referred to as the threshold voltage. A practical micropump is fabricated as well, where the experiment shows that the flow rate of the micropump increases with input voltage and the maximum value is 5.4 ml min⁻¹ while the input voltage equals 100 V. Compared with other valve-less micropumps [17, 20], this micropump has a higher output flow rate, which is even comparable to some valve micropumps [21, 22].

2. Principle of the virtual valve micropump

Figure 1(a) shows the entire structure of a typical valve-less micropump. In previous studies, many researchers believed that the diffuser/nozzle structure, shown in figure 1(b), is the key part of the valve-less micropump needed to produce unidirectional flow [23]. Olsson *et al* [13, 14, 24] propose that the diffuser/nozzle transforms kinetic energy (in the form of flow velocity) into potential energy (in the form of pressure). Since the diffuser has a low velocity in the outlet and low pressure loss, the fluid velocity decreases with static pressure gradually recovering in the diffuser direction. The nozzle, however, shows opposite behaviors. The fluid flow thus encounters lower flow resistance in the diffuser direction than the nozzle direction. The flow resistance coefficient is used to describe the flow resistance of the diffuser/nozzle [15], which is given by the following equation:

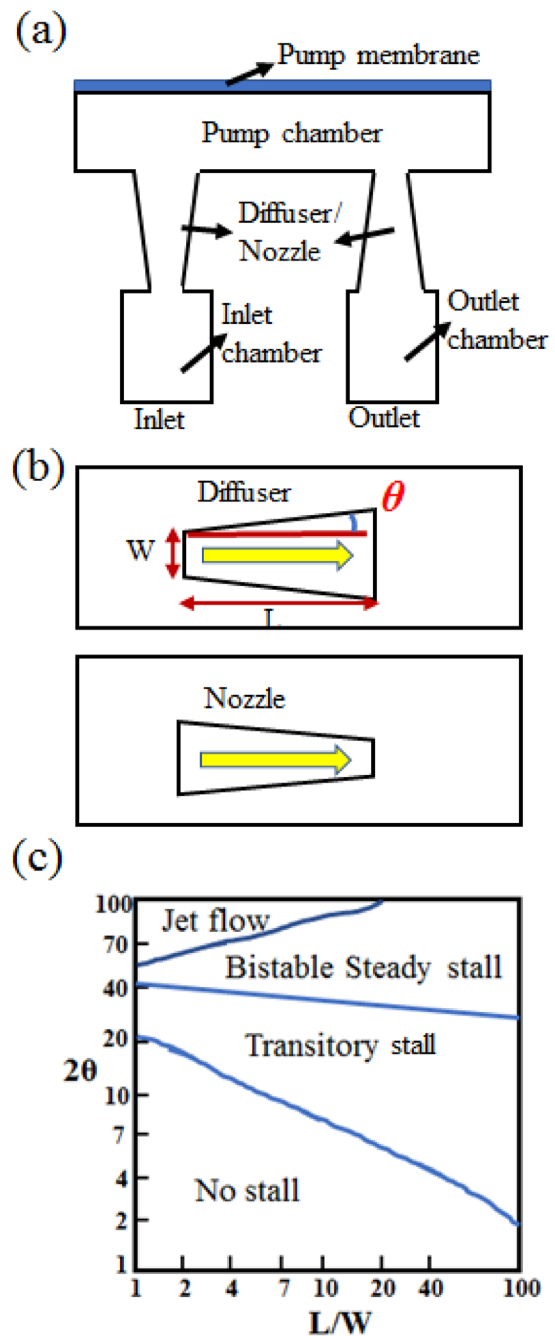


Figure 1. (a) Schematic of a typical valve-less micropump with diffuser/nozzle; (b) a typical diffuser and a typical nozzle; and (c) stability map of a diffuser plotting diffuser dimensions versus diffuser angle.

$$K = \frac{\Delta P}{\rho v^2 / 2} \quad (1)$$

where ρ is the fluid density, ΔP is the pressure drop along diffuser/nozzle, and v is the mean flow velocity of at the neck of nozzle/diffuser.

A typical diffuser has a lower pressure loss coefficient in the forward direction compared to the reverse direction. The diffuser efficiency is given by:

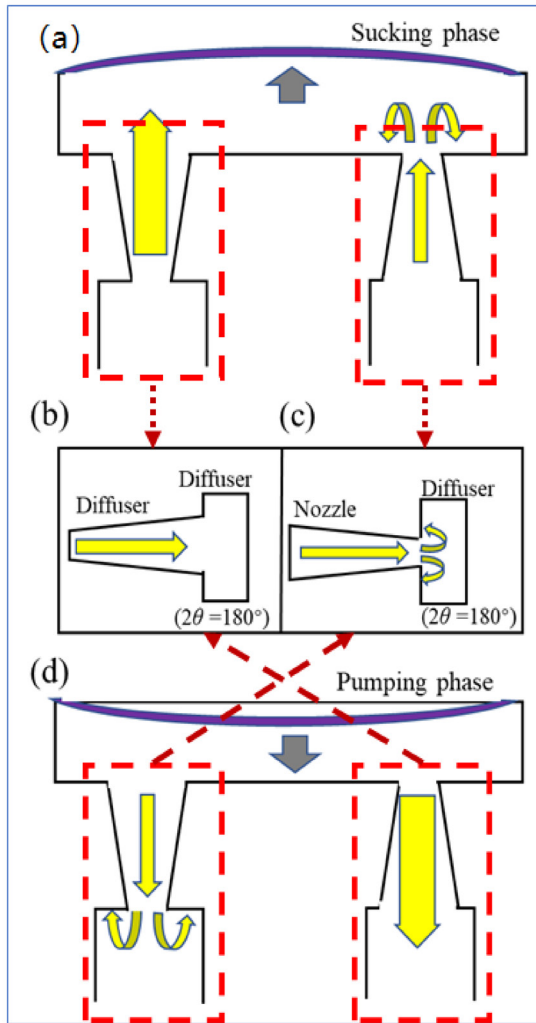


Figure 2. (a) Valve-less micropump in sucking phase; (b) two diffusers connected in series; (c) a nozzle connected with a diffuser; and (d) valve-less micropump in pumping phase.

$$\eta = \frac{K_r}{K_f} \quad (2)$$

where K_r and K_f are the pressure loss coefficients in the reverse and forward directions, respectively [16, 17]. When $\eta > 1$, the pressure loss in the forward direction is less than the pressure loss in the reverse direction, which leads to a net flow. Wei *et al* [17] report a stability map for the diffuser and summarize its fluidic characteristics, as shown in figure 1(c). Researchers point out that the diffuser should work in a transitory stall region to achieve minimum pressure drop. If 2θ is greater than 55° and fluid flows through the diffuser with a high speed, the diffuser falls into the jet flow region and has extremely poor performance.

Obviously, all the above-mentioned results are based on the diffuser/nozzle structure only. However, the surrounding components of the diffuser/nozzle also contribute to the fluidic behaviors. As shown in figure 2(a), when the micropump is in the sucking phase, fluid flows from both the inlet and outlet into the pump chamber. For the inlet, the diffuser and pump chamber are equivalent to two diffusers connected in series

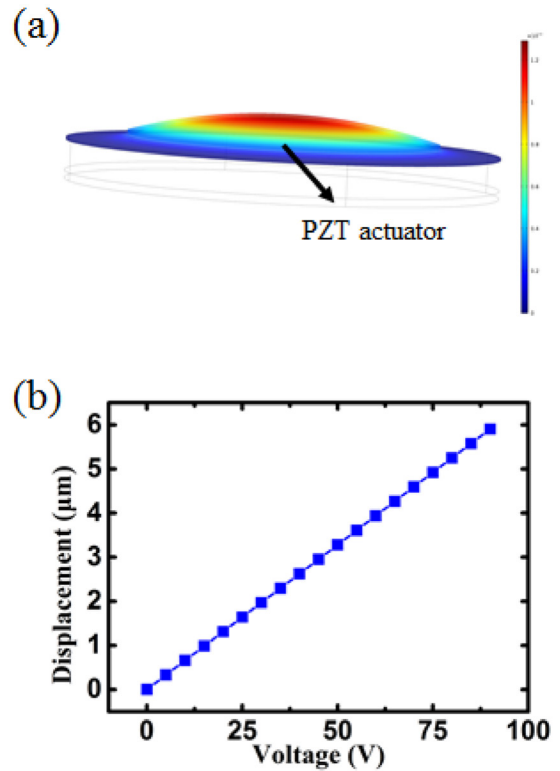


Figure 3. (a) The PZT actuator deflection under electronic force; and (b) the curve of displacement versus voltage.

(shown in figure 2(b)). The fluid's velocity starts reducing at the first diffuser and is further reduced at the second diffuser. The fluid thus faces a very small pressure drop and flows into the pump chamber with low resistance. For the outlet, the nozzle and pump chamber are equivalent to a nozzle connected with a large angle diffuser (shown in figure 2(c)). The fluidic velocity continues increasing along the first nozzle and reaches its maximum at the entrance of the second diffuser. Because the second diffuser angle equals 180° , such a diffuser works in the jet flow region. A significant vortex is generated in the second diffuser, leading to extremely poor fluid transport performance. The fluid from the outlet thus encounters large flow resistance, which can hardly flow into the chamber. As a consequence, the fluid flowing from the inlet into the pump chamber is much larger than that from the outlet. Similarly, as illustrated in figure 2(d), when the micropump is in the pumping phase, the volume of fluid flowing out from the pump chamber through the outlet is greater than that through the inlet.

3. Numerical simulation

To investigate the behaviour of the virtual valve micropump in detail, dynamic multi-physics FEM is built. The piezoelectric actuator is first studied using an electric-mechanical coupling model. As shown in figures 3(a) and (b), the maximum displacement of the piezoelectric actuator occurs at the center, and is proportional to the input voltage.

Figure 4(a) shows the transient responses of the piezoelectric actuator, where phase delay can be observed between

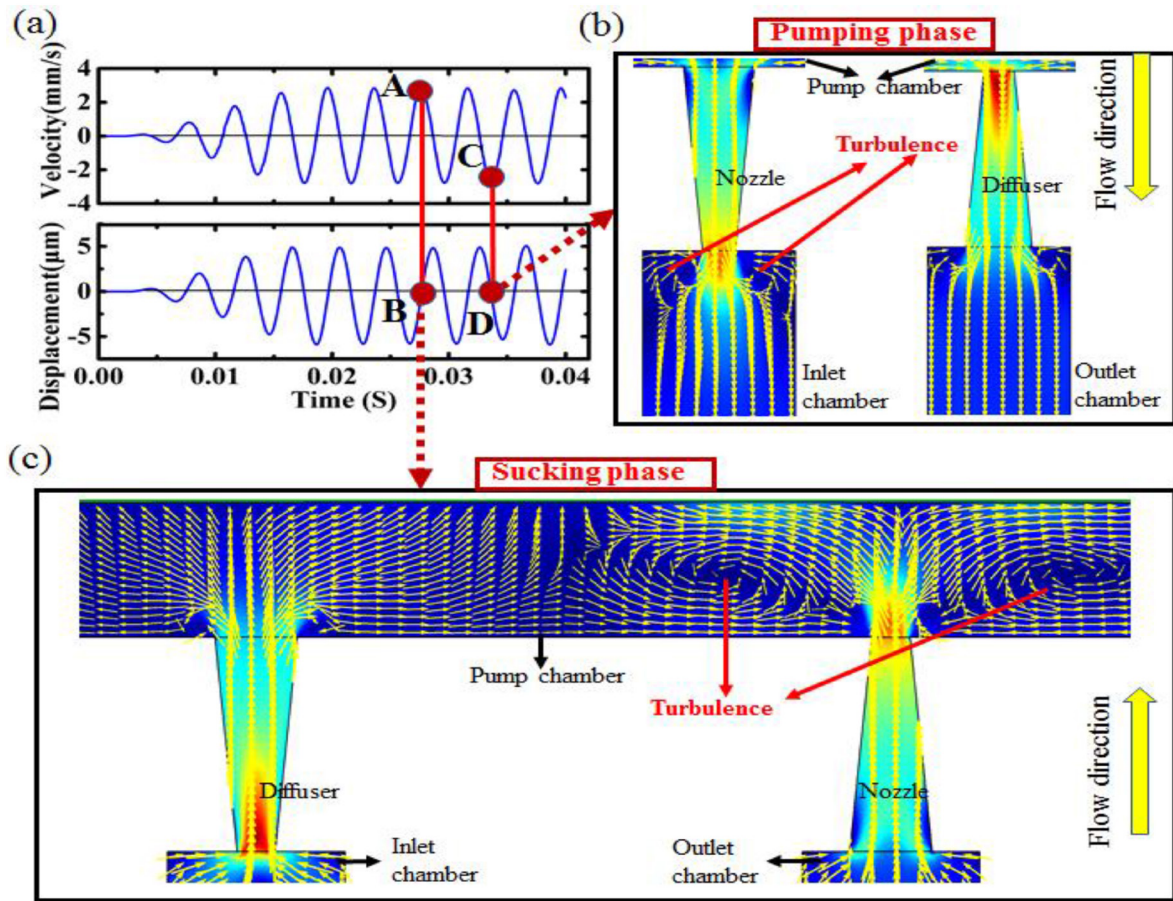


Figure 4. (a) The curve of displacement and velocity of membrane versus time; (b) the fluid velocity field of the micropump in pumping mode; and (c) the fluid velocity field of the micropump in suction mode.

the velocity and displacement. When the velocity curve reaches the peak value (point A), the sign of displacement changes from negative to positive (point B). The micropump is in the sucking phase at this time. On the contrary, when the velocity curve reaches the minimum value (point C), the sign of the displacement curve changes from positive to negative (point D), and the micropump is in the pumping phase.

The fluidic characteristics of the valve-less micropump are then studied using the fluid-structure interaction (FSI) model, where the extracted displacement of the piezoelectric actuator is input as the boundary condition. As shown in figure 4(c), when the micropump is in the sucking phase, fluid flows from both the inlet and outlet into the pump chamber; yellow arrows indicate the flowing direction of the fluid. When the fluid flows from the inlet to the pump chamber, the diffuser and pump chamber are equal to that of two connected diffusers. The fluid encounters small resistance. At the same time, when the fluid flows from the outlet to the pump chamber, the nozzle and pump chamber are equal to when a nozzle connects with a large angle diffuser. The velocity of fluid increases along the constricted nozzle direction and reach a large value at the end of the nozzle. Due to the diffuser angle equaling 180°, it is located in the jet flow region, and a high velocity fluid will generate a vortex in this region. Therefore, the fluid encounters large resistance. In general, the volume of

fluid that flows into the pump chamber from the inlet is greater than the volume that flows from the outlet. Similarly, when the micropump is in the pumping phase (as shown in figure 4(b)), fluid flows from the pump chamber to the inlet and outlet. For the same reason, the fluid flowing out through the outlet has a larger volume than that flowing out through the inlet. As the micropump working state ranges from sucking mode to pumping mode periodically, the micropump will generate net flow. The simulation result shows that the vortex emerges in the interfacial area of the nozzle end and the chamber is key to obstruct the fluid flow through the nozzle. It has the function equivalent to a valve, because the valve is not real, it is called a virtual valve.

The normalized net flow rate with time is illustrated in figure 5(a). The definition of net flow rate is given by the following equation:

$$V_{net} = V_{out} - V_{in} \tag{3}$$

where V_{in} and V_{out} are the volumetric flow rate through the inlet and outlet, respectively. As shown in figure 5(a), when the micropump works in a stable state, the net flow rate always has a positive sign. This implies such a micropump always pumps fluid forwards, and the reflux is suppressed very well with the help of the virtual valve. The accumulated output fluidic volume is defined as:

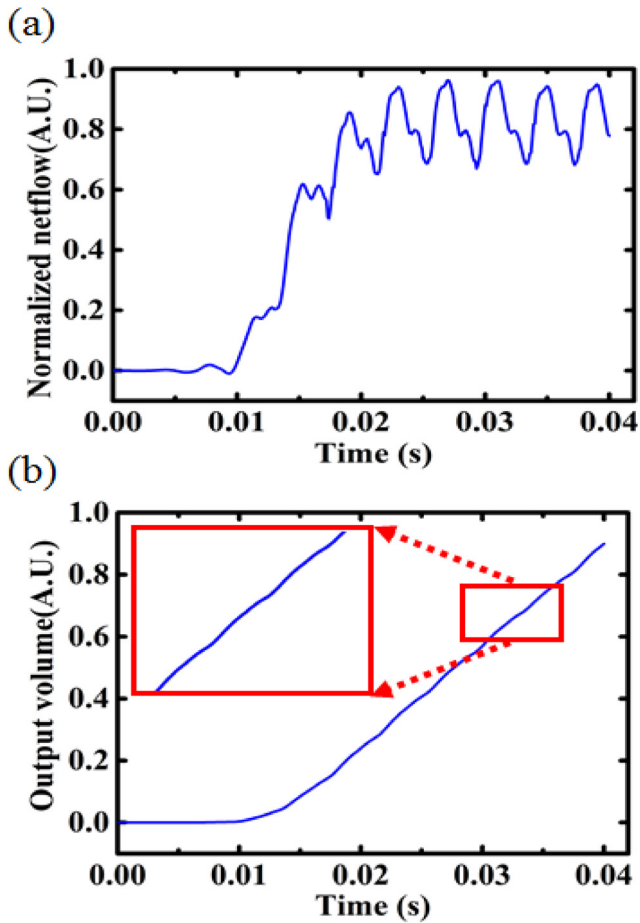


Figure 5. (a) The curve of normalized net flow (A.U.); and (b) the curve of output volume (A.U.).

$$V_{\text{pump}} = \frac{1}{2} \int_0^t V_{\text{net}} dt. \quad (4)$$

Figure 5(b) shows the accumulated output fluidic volume with respect to time. When the micropump works in the stable state, the output volume linearly increases with time. Small fluctuations can be observed from the enlarged view of figure 5(b), but the accumulated output volume keeps growing without any reduction. This high pumping efficiency, i.e. no obvious reflux can be observed, is mainly attributed to the positive net flow rate.

As is discussed above, a vortex appears in the interfacial area of the nozzle end and the chamber is considered as the key for blocking reflux. The vortex is highly related to the fluidic velocity, which is mainly determined by the micropump membrane displacement and input voltage. Hence, the input voltage (V) may largely influence the micropump’s performance.

The simulated dynamic flow details are shown in figure 6(a), under different input voltages ($V = 10, 20$ and 75 V). It clearly shows that the vortex emerges in the interfacial region of the nozzle end and inlet, and the vortex degree increases with voltage. When V equals 10 V, there is hardly

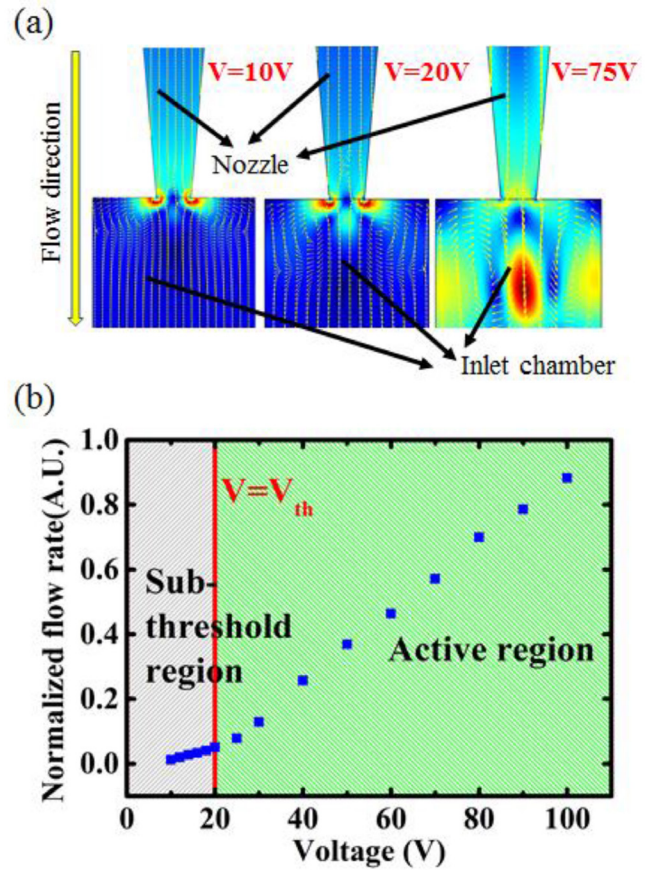


Figure 6. (a) The velocity fields of the nozzle and inlet channel of the micropump in the pumping mode plot by simulations when the input voltage $V = 10, 20$ and 75 V; and (b) the simulation flow rate of the micropump with input voltage (A.U.).

any vortex emerging in the inlet, and the reflux flows through the inlet smoothly. When V is increased to 20 V, a small vortex emerges in the inlet chamber. A significant vortex appears in the inlet when V equals 75 V. Under such an input voltage, the reflux from the nozzle is blocked very well. Figure 6(b) shows the simulated flow rate of the micropump with input voltage. The flow rate increases with the input voltage; however, the slope of the curve starts changing from $V = 20$ V. When $V < 20$ V, the slope is relatively small, while the flow rate largely increases when $V > 20$ V.

Hence, this curve can be divided into two regions: the sub-threshold region and the active region (as shown in figure 6(b)). When the voltage is located in the subthreshold region, the actuator membrane has small displacement, and the fluid flows through the nozzle slowly. No vortex emerges and the micropump works in the normal low-efficient state. However, when the voltage is located in the active region, the vortex emerges at the interface of the nozzle end and the chamber largely blocks the reflux. The virtual valve is activated in this region, resulting in high pumping efficiency. Therefore, voltage seems to be the key parameter which activates the virtual valve, and 20 V is referred to as the threshold voltage. It is worth noting that the threshold voltage is not a constant, but should be determined by the micropump’s design.

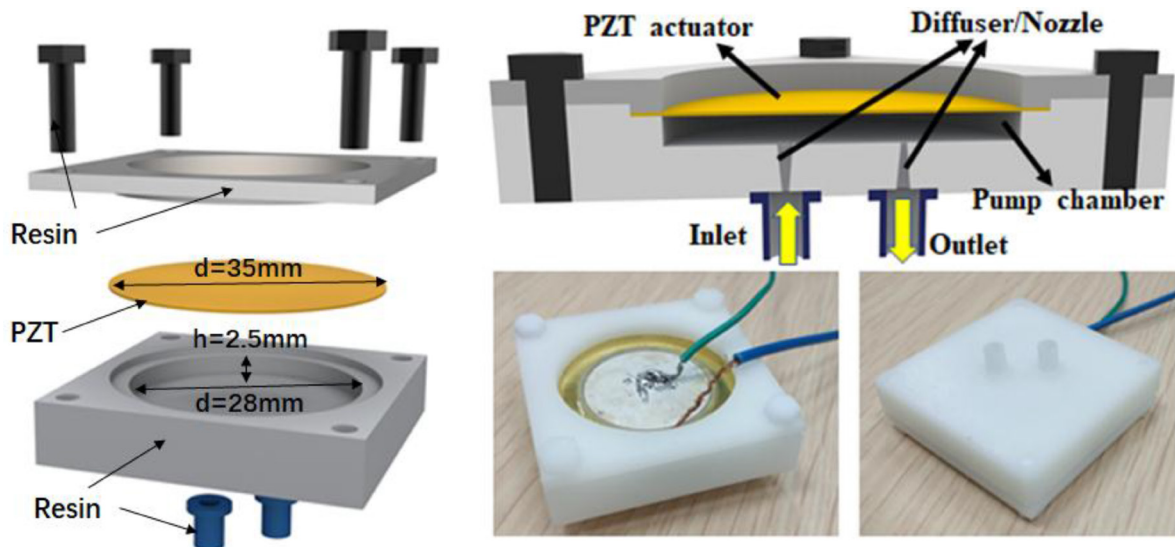


Figure 7. Schematic diagram of the valve-less micropump, cross-sectional view, and photograph of the fabricated micropump.

4. Device fabrication and experimental setup

A practical valve-less micropump is fabricated with 3D printing technology based on the simulation results, where the 3D drawing is shown in figure 7. The valve-less micropump consists of a pump chamber (where the diameter is 28 mm, and the height is 2.5 mm), a lead zirconate titanate (PZT) ceramic-based actuator (the diameter is 35 mm), inlet channel and outlet channel. For the nozzle/diffuser, the narrow radius is 0.5 mm, the wide radius is 1.2 mm, and the length of the nozzle/diffuser is 3 mm. Except for the actuator, all of the pump is made by resin. After the micropump is fabricated, an experimental setup is used to measure the flow rate of the micropump [25], which consists of a function generator, a DRV2700EVM amplifier, a micropump, plastic pipes, deionized water and so on [1, 26]. The micropump is driven by the amplified sinusoidal electrical signal, and a bias voltage is also imposed on the piezoelectric actuator to protect the actuator from breakdown. The delivered volumetric flow rate is calculated by measuring the moving distance of the liquid surface in a certain tube for a given time [26].

5. Experimental results and discussions

By changing the input voltage amplitude from 0 to 100 V, the curve of flow rate versus voltage is plotted in figure 8(a). It clearly shows that the curve has different slopes for $V < 20$ V and $V > 20$ V. When $V < 20$ V, the curve has a small slope. However, when $V > 20$ V, the flow rate of the micropump rapidly increases with input voltage, and 5.4 ml min^{-1} is finally achieved at 100 V. Previously reported valve-less micropumps usually have low output flow rates. A valve-less micropump with a maximum flow rate of 1.2 ml min^{-1} at a driving voltage of 160 V is reported by Tseng [20]. Wei [17] designed a micropump which has a flow rate of $38 \mu\text{l min}^{-1}$. In terms of the valve micropump, the micropump described in this paper has a higher pumping efficiency than the valve-less micropump.

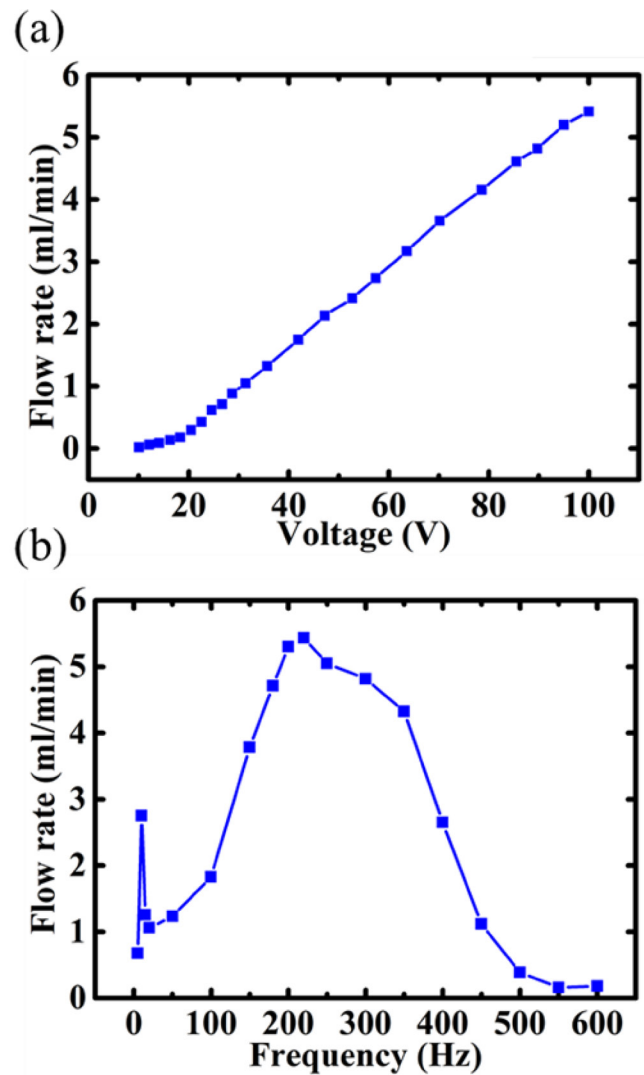


Figure 8. (a) The experimental flow rate of the micropump with input voltage (ml min^{-1}); and (b) the experimental flow rate of the micropump with input frequency (ml min^{-1}).

Table 1. Flow rate comparison of the reported micropumps.

Micropump type	Chamber diameter (mm)	Chamber volume (mm ³)	Driving voltage (V)	Flow rate (ml min ⁻¹)	Researchers
Valve-less	15	88.31	80	0.038	Wei <i>et al</i> [17]
Valve-less	8	3.52	160	1.2	Tseng <i>et al</i> [20]
Valve	10	117.75	80	6.2	Ma <i>et al</i> [21]
Valve	35	384.65	150	3.12	Zhang <i>et al</i> [22]
Virtual valve	28	1538.6	100	5.4	This paper

The flow rate of a separable valve micropump proposed by Ma *et al* can reach a maximum of 6.21 ml min⁻¹ at voltage of 80 V [21]. Zhang presents a valve micropump achieving a maximum flow rate of 3.12 ml min⁻¹ at 21 Hz with a driving voltage of 150 V [22]. The flow rates of the micropumps are compared with respect to the chamber dimensions, listed in table 1. With the help of the virtual valve, the valve-less micropump proposed in this paper has a considerably high flow rate, and such output flow rate is already comparable to some valve micropumps. Figure 8(b) shows the measured flow rate curve with frequency. The maximum volumetric flow rate is achieved at a frequency of 220 Hz, where the displacement of the piezoelectric actuator also reaches its maximum.

6. Conclusion

In conclusion, dynamic FEM for studying the mechanism of a valve-less micropump has been developed in this research. We investigated the fluidic behavior in the micropump and its relationship to pumping performance. The simulation result shows that the flow performance of the valve-less micropump is not only dependent on the diffuser/nozzle but also related to the entire structure. When fluid flows through the nozzle, the chamber which is in contact with the nozzle end is considered as a diffuser with an angle of 180°. The fluid generates a vortex in the interface area of the nozzle end and chamber, and such a vortex is equivalent to a virtual valve, which can restrict the reflux. Furthermore, it is found that the micropump membrane with a higher input voltage leads to a larger fluidic velocity, resulting in higher vortex degree. Therefore, the vortex degree is closely related to the input voltage amplitude. When the input voltage is larger than the threshold voltage ($V = 20$), the vortex starts emerging, and the flow rate of the micropump rapidly increases with input voltage. The experimental results are consistent with the simulation results, and a high output flow rate of 5.4 ml min⁻¹ is finally achieved, which is comparable to a typical valve micropump.

Acknowledgments

This work was supported by the National Natural Science Foundation of China (No. 51602039) and Central University

Support Project (ZYGX2017, KYQD160, ZYGX2016J051 and ZYGX2016J050).

ORCID iDs

Tao Wang  <https://orcid.org/0000-0001-8453-535X>

Chengkuo Lee  <https://orcid.org/0000-0002-8886-3649>

References

- [1] Jiang L 2012 The dynamic characteristics of a valve-less micropump *Chin. Phys. B* **21** 363–71
- [2] Chen S *et al* 2015 The structure of wheel check valve influence on air block phenomenon of piezoelectric micropump *Micromachines* **6** 1745–54
- [3] Cheng L 2007 Manufacture of three-dimensional valveless micropump *J. Mater. Process. Technol.* **192–3** 229–36
- [4] Dau D 2015 Numerical study and experimental validation of a valveless piezoelectric air blower for fluidic applications *Sensors Actuators B* **221** 1077–83
- [5] Karmozdi M, Salari A and Shafii M B 2013 Experimental study of a novel magneto mercury reciprocating (MMR) micropump, fabrication and operation *Sensors Actuators A* **194** 277–84
- [6] Benaissa A and Belkhiat S 2012 Performances analysis of a piezo-pump *EPJ Web Conf.* **29** 00007
- [7] Stemme S 1993 A valveless diffuser/nozzle-based fluid pump *Sensors Actuators A* **39** 159–67
- [8] Gerlach T 1998 Microdiffusers as dynamic passive valves for micropump applications *Sensors Actuators A* **69** 181–91
- [9] Ullmann A, Fono I and Taitel Y 2001 A piezoelectric valve-less pump-dynamic model *J. Fluids Eng.* **123** 92–98
- [10] Nakahara K *et al* 2013 A peristaltic micropump using traveling waves on a polymer membrane *J. Micromech. Microeng.* **23** 085024
- [11] Yamahata K *et al* 2005 A PMMA valveless micropump using electromagnetic actuation *Microfluid. Nanofluidics* **1** 197–207
- [12] Olsson A, Stemme G and Stemme E 2000 Numerical and experimental studies of flat-walled diffuser elements for valve-less micropumps *Sensors Actuators A* **84** 165–75
- [13] Ullmann A 1998 The piezoelectric valve-less pump—performance enhancement analysis *Sensors Actuators A* **69** 97–105
- [14] Olsson A *et al* 1996 A valve-less planar pump isotropically etched in silicon *J. Micromech. Microeng.* **6** 87–91

- [15] Jiang X N *et al* 1998 Micronozzle/diffuser flow and its application in micro valveless pumps *Sensors Actuators A* **70** 81–7
- [16] Singhal V, Garimella S V and Murthy J Y 2004 Low Reynolds number flow through nozzle-diffuser elements in valveless micropumps *Sensors Actuators A* **113** 226–35
- [17] Wei Y *et al* 2014 A novel fabrication process to realize a valveless micropump on a flexible substrate *Smart Mater. Struct.* **23** 025034
- [18] Olsson A, Stemme G and Stemme E 1995 A valve-less planar fluid pump with 2 pump chambers *Sensors Actuators A* **47** 549–56
- [19] Gerlach T and Wurmus H 1995 Working principle and performance of the dynamic micropump *Sensors Actuators A* **50** 135–40
- [20] Tseng L-Y *et al* 2013 Investigation of a piezoelectric valveless micropump with an integrated stainless-steel diffuser/nozzle bulge-piece design *Smart Mater. Struct.* **22** 085023
- [21] Ma H-K, Luo W-F and Lin J-Y 2015 Development of a piezoelectric micropump with novel separable design for medical applications *Sensors Actuators A* **236** 57–66
- [22] Zhang Z *et al* 2016 Development of a self-sensing piezoelectric pump with a bimorph transducer *J. Intell. Mater. Syst. Struct.* **27** 581–91
- [23] Jeong J and Kim C N 2007 A numerical simulation on diffuser-nozzle based piezoelectric micropumps with two different numerical models *Int. J. Numer. Methods Fluids* **53** 561–71
- [24] Tsui Y-Y and Lu S-L 2008 Evaluation of the performance of a valveless micropump by cfd and lumped-system analyses *Sensors Actuators A* **148** 138–48
- [25] Cazorla P-H *et al* 2016 A low voltage silicon micro-pump based on piezoelectric thin films *Sensors Actuators A* **250** 35–9
- [26] Chandika S, Asokan R and Vijayakumar K C K 2012 Flow characteristics of the diffuser/nozzle micropump—a state space approach *Flow Meas. Instrum.* **28** 28–34